THE JOURNAL OF PHYSICAL CHEMISTRY C
A JOURNAL OF THE AMERICAN CHEMICAL SOCIETY

pubs.acs.org/JPCC

Article

1-Bromopropane Capture with Hydrophobic Zeolites: Force Field Development and Molecular Simulations

A. Ozgur Yazaydin*

Cite This: J. Phys. Chem. C 2022, 126, 5728−5734

Read Online

ACCESS | Metrics & More | Article Recommendations | Supporting Information

ABSTRACT: 1-Bromopropane is a solvent used in various industrial and commercial applications. United States Environmental Protection Agency recently concluded that 1-bromopropane posed unreasonable risks to human health in several conditions of use. In this work, the adsorption of 1-bromopropane vapors in zeolites was investigated using molecular simulations. First, a united-atom model of 1-bromopropane was developed and the model was validated to reproduce vapor−liquid equilibrium properties of 1-bromopropane by carrying out Gibbs ensemble Monte Carlo simulations. The new model was then used to investigate the capture of 1-bromopropane in hydrophobic zeolites with Monte Carlo simulations in the grand canonical ensemble. The results show that a filtering system that consists of MRE and STW zeolites can capture 1-bromopropane within its ambient concentration range that occurs as a result of 1-bromopropane release in various industrial and commercial applications as identified by the US EPA. While MRE zeolite has the optimal pore size that provides favorable host−guest interactions to capture 1-bromopropane at extremely low concentrations, rapid condensation of 1-bromopropane occurs at relatively higher concentrations in the intersections of narrow helical and straight pores in the STW zeolite.

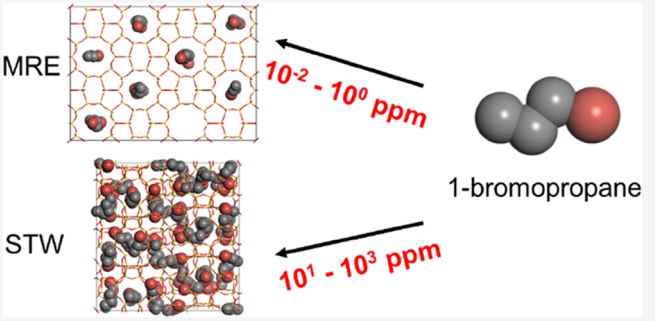

1. INTRODUCTION

1-Bromopropane, also known as n-propyl bromide, is a brominated hydrocarbon that is used in various industrial, commercial, and consumer applications. It is a colorless liquid with a sweet odor and is slightly soluble in water. 1-Bromopropane is considered a volatile organic compound (VOC) that exhibits high volatility, low boiling point, low flammability, and no explosivity.[1] Common uses of 1-bromopropane include the dry cleaning solvent, spot cleaner, stain remover, spray adhesive for foam cushion manufacturing, engine degreaser, brake cleaner, automotive refrigerant flush, degreaser for computer, electronic, and electrical products, asphalt extraction, and adhesive accelerant for arts, crafts, and hobby materials.[2]

The use of 1-bromopropane has increased after it was identified as an environmentally friendly replacement for ozone-depleting solvents, as well as in response to the restricted use of tetrachloroethylene in the dry cleaning industry.[3] On the other hand, several human and animal studies reported the neurotoxicity, reproductive toxicity, and hepatotoxicity of 1-bromopropane and the consequent adverse health effects.[4−9]

In its final risk evaluation report for 1-bromopropane published in August 2020, the United States (US) Environmental Protection Agency (EPA) concluded that 1-bromopropane posed unreasonable risks to human health in 16 out of 25 conditions of use they investigated. This included unreasonable risks to the health of workers who are in direct contact with 1-bromopropane, as well as to those who work nearby, which can be due to both short- and long-term inhalation exposure. EPA's report has also identified unreasonable risks to the health of consumers and bystanders due to short-term inhalation and dermal exposure.[10]

Zeolites are microporous crystalline materials that consist of linked TO_4 tetrahedra, where the T is usually Si or Al, which forms three-dimensional frameworks with well-defined pores of molecular dimensions. Zeolites can be used in face masks or in air purification systems to capture 1-bromopropane from air and prevent its inhalation and dermal exposure. In this study, using molecular simulations, the adsorption of 1-bromopropane vapors in zeolites was investigated. First, a force field that reproduces the phase equilibrium properties of 1-bromopropane was parameterized. Then, zeolites were screened for the adsorption of 1-bromopropane to identify materials that can be used to capture 1-bromopropane under the conditions of use investigated by US EPA.

Received: January 5, 2022
Revised: March 1, 2022
Published: March 18, 2022

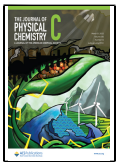

2. COMPUTATIONAL METHODS

Classical force-field-based molecular simulations were carried out with the RASPA molecular simulation software[11] to predict phase equilibrium properties of 1-bromopropane and its adsorption in zeolites. In these simulations, short-range van der Waals interactions and long-range electrostatic interactions between nonbonded atoms were computed using a combination of Lennard-Jones (LJ) and Coulomb potentials, respectively

$$U_{\text{non-bonded}} = 4\varepsilon_{ij}\left(\left(\frac{\sigma_{ij}}{r_{ij}}\right)^{12} - \left(\frac{\sigma_{ij}}{r_{ij}}\right)^{6}\right) + \frac{q_i q_j}{4\pi\varepsilon_0 r_{ij}}$$

where i and j are interacting atoms and r_{ij} is the distance between atoms i and j. ε_{ij} and σ_{ij} are the LJ well depth and diameter, respectively. q_i and q_j are the partial charges of the interacting atoms and ε_0 is the dielectric constant. LJ parameters between different atom types were calculated using the Lorentz−Berthelot mixing rules. The cut-off distance for LJ interactions was 14.0 Å with tail corrections applied. The Ewald sum method was employed to compute electrostatic interactions.

2.1. 1-Bromopropane Model. To carry out accurate molecular simulations of 1-bromopropane, a united-atom model of the 1-bromopropane molecule is developed. In this model, hydrogen atoms and the carbon atom that they are bonded to, i.e., CH_3 and CH_2, are considered as a single united atom (Figure 1). Bonds that connect the two atoms are kept at a fixed

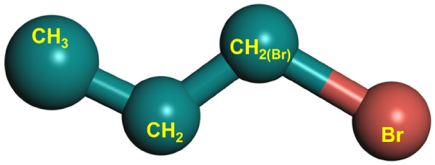

Figure 1. United-atom model of 1-bromopropane.

length. The angle bending between three atoms is represented by a harmonic potential

$$U_{\text{bend}} = \frac{1}{2}k_\theta(\theta - \theta_0)$$

where k_θ is the force constant and θ_0 is the equilibrium angle. The motion of the dihedral angle φ is governed by the OPLS united-atom torsional potential

$$U_{\text{tors}} = c_1[1 + \cos\varphi] + c_2[1 - \cos(2\varphi)] + c_3[1 + \cos(3\varphi)]$$

The parameters for the LJ potential and the bonded potentials were taken from the TraPPE[12] or OPLS[13−15] force fields. However, partial charges of the CH_3 and CH_2 united atoms and the Br atom of the 1-bromopropane molecule were derived from quantum chemical calculations. For this purpose, first, a 1-bromopropane molecule was geometry-optimized using the Gaussian09[16] software at MP2 level of theory and with the 6−311+g(d) basis set. Then, partial atomic charges were fitted with the ChelpG method[17] to the electrostatic potential obtained from the quantum chemical calculation (Figure S1). The partial charges for the united atoms were finalized by summing the partial charges of the hydrogen atoms and the partial charge of the carbon atom that they are bonded to.

All force field parameters for the united-atom model of 1-bromopropane developed in this work are given in Table 1. To

Table 1. Force Field Parameters of the 1-Bromopropane United-Atom Model

parameters for nonbonded potentials				
atom type	q (e)[a]	ε/k_B (K)	σ (Å)	refs[b]
CH_3	−0.106	98.0	3.75	12
CH_2	0.246	46.0	3.95	12
$CH_{2(Br)}$	0.085	46.0	3.95	12
Br	−0.225	250.0	3.47	[a]
parameters for bonded potentials				
fixed bond	length (Å)			refs
CH_3−CH_2	1.54			12
CH_2−$CH_{2(Br)}$	1.54			12
$CH_{2(Br)}$−Br	1.945			14
angle bend	k_θ/k_B (K/rad^2)		θ_0 (deg)	refs
CH_3−CH_2−$CH_{2(Br)}$	62,500		114	12
CH_2−$CH_{2(Br)}$−Br	69,445		110	14
torsion	c_1/k_B (K)	c_2/k_B (K)	c_3/k_B (K)	refs
CH_3−CH_2−$CH_{2(Br)}$−Br	335.03	−68.19	791.32	12

[a]This work. [b]References for LJ parameters only.

validate the model, Gibbs ensemble Monte Carlo (GEMC)[18,19] simulations were carried out to compute phase equilibrium properties of 1-bromopropane and the results were compared against the experimental data. In GEMC simulations, there are two simulation boxes. The temperature and the total volume of the two boxes and the total number of molecules are fixed; however, the two boxes exchange volume between each other and molecules are transferred from one box to the other, so the volume and the number of molecules in each box fluctuate during a GEMC simulation. In total, there were 300 1-bromopropane molecules in the two boxes. Translation, rotation, reinsertion, partial regrowth and transfer of 1-bromopropane molecules, and volume exchange between two boxes were sampled with probabilities of 34, 34, 5, 5, 20, and 2%, respectively. The transfer of 1-bromopropane molecules from one box to another was sampled with the continuous fractional component (CFC) method,[20−22] which increases the acceptance rate of the transfer of a molecule. This is particularly useful for the transfer of a 1-bromopropane molecule from the vapor box to the liquid box. CFC works by coupling the strength of the interaction of a molecule with the rest of the system with a continuous fractional parameter, λ, which varies between 0 and 1. The closer λ is to 0, the weaker the interaction between the molecule and the rest of the system, whereas, the closer the λ is to 1, the stronger the interaction of the molecule with the rest of the system. Between λ = 0 and 1, the molecule is a so-called fractional molecule. At λ = 1, the molecule is a whole molecule and is considered to have been inserted to the system; i.e., the number of molecules in the simulation box increases by one. At λ= 0, the molecule does not interact with the rest of the system and is considered to have been deleted; i.e., the number of molecules in the simulation box decreases by one. Introducing the parameter λ adds an additional degree of freedom to the system. When a fractional molecule is inserted to the system, λ is randomly determined and the succeeding changes in λ are sampled with a Monte Carlo trial move. Biasing of λ is required to avoid the system from getting trapped at certain values of λ. This is done using a weight function, W(λ), which can be obtained via the Wang−Landau algorithm.[16] Each GEMC simulation was first equilibrated for 100,000 cycles. A cycle is N steps, where N is equal to the number of molecules in the system.

https://doi.org/10.1021/acs.jpcc.2c00086
J. Phys. Chem. C 2022, 126, 5728−5734

This was followed by another 100,000 cycles to compute the biasing function $W(\lambda, i)$ to obtain a flat probability distribution of λ. Finally, a 100,000 cycle production run was carried out from which saturated vapor and liquid densities and vapor pressures of 1-bromopropane were averaged and reported.

2.2. Zeolite Models. The model structures of zeolites considered in this study were based on their crystallographically determined structures as described in the Database of Zeolite Structures prepared by the International Zeolite Association (IZA)'s structure commission.[23] At the time of this study, there were 253 zeolite topologies reported in the aforementioned database. Among them, 16 topologies (CHI, CLO, EWT, IFT, IFU, IRY, ITN, ITV, LIT, PAR, RON, SSO, SVR, SVT, SVY, and WEN) were not considered as in these topologies the framework is interrupted; i.e., not all T atoms are 4-connected. The remaining 237 topologies were modeled as rigid frameworks in their siliceous form. The LJ parameters and the partial charges of the zeolite atoms were taken from the TraPPE-zeo force field[24] and are listed in Table S1.

2.3. Structural Screening. An initial screening of the zeolite structures was carried out based on pore limiting diameter (PLD) using the PoreBlazer v4.0 code.[25] PLD is defined as the maximum penetrant diameter where a pore network remains percolated. Zeolites with a PLD greater than 4.0 Å were considered for adsorption simulations of 1-bromopropane.

2.4. Adsorption Simulations. Adsorption isotherms of 1-bromopropane in zeolites at 20 °C were computed by carrying out grand canonical Monte Carlo (GCMC) simulations. In the grand canonical ensemble, the temperature, volume, and chemical potential of the system are fixed; however, the number of molecules in the system fluctuate. Translation, rotation, reinsertion, partial regrowth, and insertion/deletion of the 1-bromopropane molecule were sampled with probabilities of 33, 33, 5, 5, and 25%, respectively. The insertion/deletion of 1-bromopropane molecules was sampled with the CFC method.[20−22] This was particularly useful to increase the efficiency of the insertion 1-bromopropane molecules into the pores of the zeolites. Fugacity of 1-bromopropane, which is required as part of the acceptance rule for the insertion/deletion moves,[26] was calculated using the Peng−Robinson equation of state.[27] The unit cells of the zeolite were replicated such that the shortest side of the simulation cells was at least twice the cut-off distance. Each GCMC simulation was first equilibrated for 100,000 cycles. A cycle is N steps, where N is minimum 20 or equal to the number of molecules in the system. This was followed by another 100,000 cycles to compute the biasing function $W(\lambda, i)$ to obtain a flat probability distribution of λ. Finally, a 100,000 cycle production run was carried out from which adsorbed quantities of 1-bromopropane were averaged and reported.

3. RESULTS AND DISCUSSION

3.1. Validation of the 1-Bromopropane Force Field. Figure 2 shows the vapor−liquid coexistence curve (VLCC) of the 1-bromopropane united-atom model computed from the GEMC simulations. Simulated densities are in excellent agreement with the experimental data, which are only available in the liquid phase, whereas the experimental data for vapor densities of 1-bromopropane was not found in the literature. Figure 3 shows that computed saturated vapor pressures of the 1-bromopropane united-atom model are in very good agreement with the experimental data, which indicates that the model represents the vapor phase successfully.

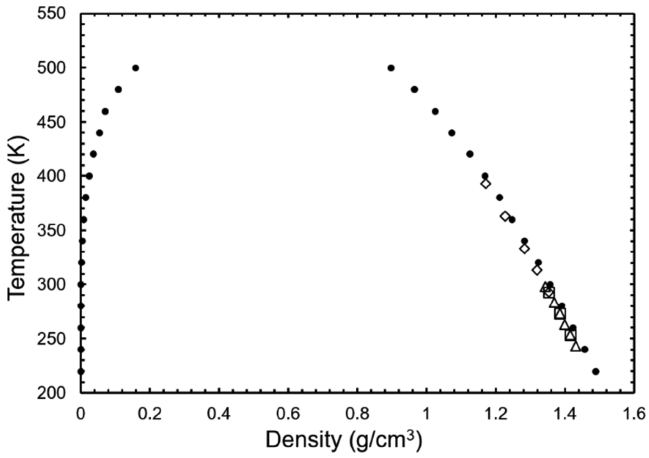

Figure 2. Vapor−liquid coexistence curve of the 1-bromopropane united-atom model (filled circles) and experimental densities: Bolotnikov et al. (triangles),[32] Rutherford et al. (diamonds),[33] and Ryshkova et al. (squares).[34] A close-up of the region where experimental densities are available is given in Figure S2 for easier comparison of the simulated and experimental data.

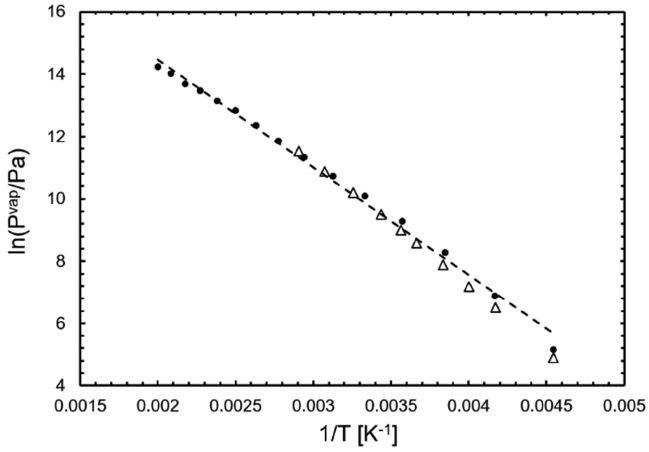

Figure 3. Clausius−Clapeyron plot of the saturated vapor pressure of the 1-bromopropane united-atom model (filled circles) and experimental data from Stull et al. (triangles).[35] The dashed line is linear fit to the simulated data. A close-up of the region where experimental densities are available is given in Figure S3 for easier comparison of the simulated and experimental data.

The critical properties of 1-bromopropane were estimated by extrapolating the subcritical data obtained from GEMC simulations using the density scaling law[28]

$$\rho_{liq} - \rho_{vap} = B(T - T_c)^{\beta}$$

for the critical temperature, T_c, using the law of rectilinear diameters[29]

$$1/2(\rho_{liq} + \rho_{vap}) = \rho_c + A(T - T_c)$$

for the critical density, ρ_c, and using the Clausius−Clapeyron equation[30]

$$\ln P = C + \frac{C'}{T}$$

https://doi.org/10.1021/acs.jpcc.2c00086
J. Phys. Chem. C 2022, 126, 5728−5734

for the critical pressure, P_c. In the above equations, ρ_{liq} and ρ_{vap} are the saturated liquid and vapor densities; T and P are the temperature and pressure (which was computed from the molecular virial[31]); A, B, C, and C' are constants, and β is the critical exponent, which is 0.32.[12] The normal boiling temperature, T_b, of the 1-bromopropane united-atom model was estimated by interpolating between the two temperatures at which the computed saturated vapor pressures were closest to 1 atm.

Table 2 gives the critical properties and the normal boiling temperature of the 1-bromopropane united-atom model estimated from the GEMC simulations data. The estimated normal boiling temperature, critical temperature, and critical density are in very good agreement with the experimental data. The estimated critical pressure, on the other hand, is about 28% lower than the experimental data. The discrepancy is largely due to the nonlinearity of the Clasius−Clapeyron plot, whereas for an accurate estimation, the enthalpy of vaporization should be independent of temperature; i.e., ln (P) vs inverse temperature plot is linear. Nevertheless, the computed saturated vapor pressures around the ambient temperature are in excellent agreement with the experimental data (Figures 3 and S3). Therefore, considering that exposure to 1-bromopropane happens at ambient conditions, i.e., $1/T$ = 0.0033 K^{-1}, the new united-atom model can be used with confidence to simulate the adsorption of 1-bromopropane in zeolites.

Table 2. Normal Boiling Point and Critical Properties of the 1-Bromopropane United-Atom Model

	simulation	experiment[36]
T_b [K]	346	344
T_c [K]	538	536.9
ρ_c [g/cm^3]	0.469	0.454
P_c [MPa]	3.13	4.33

3.2. Validation of 1-Bromopropane−Zeolite Interactions. The force-field-based interactions between 1-bromopropane and zeolites were validated against binding energies obtained from quantum chemical calculations carried out by the Gaussian09 software. Three zeolites with one-dimensional channels, MRE, AFI, and DON, with diameters around 5.6, 7.5, and 8.0 Å, respectively, were considered. To obtain the binding energy of 1-bromopropane with quantum chemical calculations, a pore channel was isolated from each zeolite and dangling oxygen atoms were terminated with hydrogen atoms; then, the 1-bromopropane molecule was geometry optimized in the channel. During the optimization calculations, zeolite atoms were fixed in their positions. Figure S4 shows the optimized positions of the 1-bromopropane molecule in the isolated channels of MRE, AFI, and DON. The computational cost of high-level quantum chemical calculations, i.e., at MP2 level of theory, was prohibitively expensive for the systems considered, as there were more than 200 atoms. Therefore, the quantum chemical optimization and binding energy calculations were carried out with the dispersion-corrected density functional theory (DFT), which employed the wB97XD functional[37] and 6−31g(d,p) basis set. The binding energy, E_B, was calculated according to the following formula

$$E_B = E_{complex} - [E_{zeolite} + E_{1-bromopropane}]$$

where $E_{complex}$ is the energy of the zeolite/1-bromopropane complex, $E_{zeolite}$ is the energy of the isolated zeolite channel, and $E_{1\text{-bromopropane}}$ is the energy of the optimized 1-bromopropane molecule. The DFT calculated binding energies were corrected for the basis set superposition error (BSSE). Table 3 shows the binding energies of 1-bromopropane obtained from DFT optimization calculations and with those obtained from force field-based energy minimization calculations carried out with RASPA. In AFI, the agreement between the force-field-based binding energy and that of computed form DFT is excellent. For MRE and DON, where the force-field-based binding energies are about 15% weaker than those computed from DFT, the agreement is relatively less satisfactory compared to AFI but still good. Overall, based on the results given in Table 3, adsorbate−adsorbent interactions were deemed to be sufficiently accurate to carry out the 1-bromopropane adsorption simulations.

Table 3. 1-Bromopropane Binding Energies in MRE and DON Zeolites

	1-bromopropane binding energy (kJ/mol)		
calculation type	MRE	AFI	DON
DFT optimization (isolated channel)	−73.8	−41.0	−51.0
force-field-based energy minimization (periodic)	−63.2	−42.1	−42.5

3.3. Adsorption of 1-Bromopropane in Zeolites. Among the 237 zeolite topologies considered, 105 of them have a PLD greater than or equal to 4.0 Å based on structural screening calculations with the PoreBlazer code.[25] Zeolites topologies with a PLD less than 4.0 Å were discarded as 1-bromopropane is not expected to diffuse into their pores. Out of the 105 zeolites with a PLD greater than or equal to 4.0 Å, 52 of them have an experimentally reported siliceous, i.e., defect-free, structure according to the IZA's database.[23] Zeolites with defects are susceptible to adsorbing significant amounts of water from humid air and not expected to capture 1-bromopropane efficiently. Therefore, GCMC simulations were carried out for 52 siliceous zeolite structures with a PLD greater than or equal to 4.0 Å.

Time-weighted average (TWA) ambient concentrations of 1-bromopropane, which workers and occupational nonusers are exposed to, range from 10^{-2} to 10^3 ppm according to the US EPA's final risk evaluation report for 1-bromopropane. This is because, depending on the application, different amounts of 1-bromopropane are released to the work environment. Ideally, it is desirable to capture 1-bromopropane using one zeolite type. However, this may not be possible given the large range of exposure concentration.

Figure 4 shows the five zeolites that have the highest absolute loading of 1-bromopropane computed by GCMC simulations at 20 °C and at partial pressures that correspond to the 1-bromopropane concentrations of 10^{-2}, 10^{-1}, 10^0, 10^1, 10^2, and 10^3 ppm at atmospheric pressure. As anticipated, for different concentrations of 1-bromopropane, the top-performing zeolites vary. At 10^{-2}, 10^{-1}, and 10^0 ppm, MRE[38] has the highest uptake. At 10^1, 10^2, and 10^3 ppm, STW[39] has the highest uptake.

To understand the high 1-bromopropane uptake in MRE and STW zeolites, their pore size distribution and geometric accessible specific surface area and pore volume were calculated with the PoreBlazer software. At low pressures, adsorbent−adsorbate interactions dominate the adsorption mechanism. This requires favorable host−guest interactions. Indeed, the high uptake performance of MRE at 10^{-2}, 10^{-1}, and 10^0 ppm 1-

https://doi.org/10.1021/acs.jpcc.2c00086
J. Phys. Chem. C 2022, 126, 5728−5734

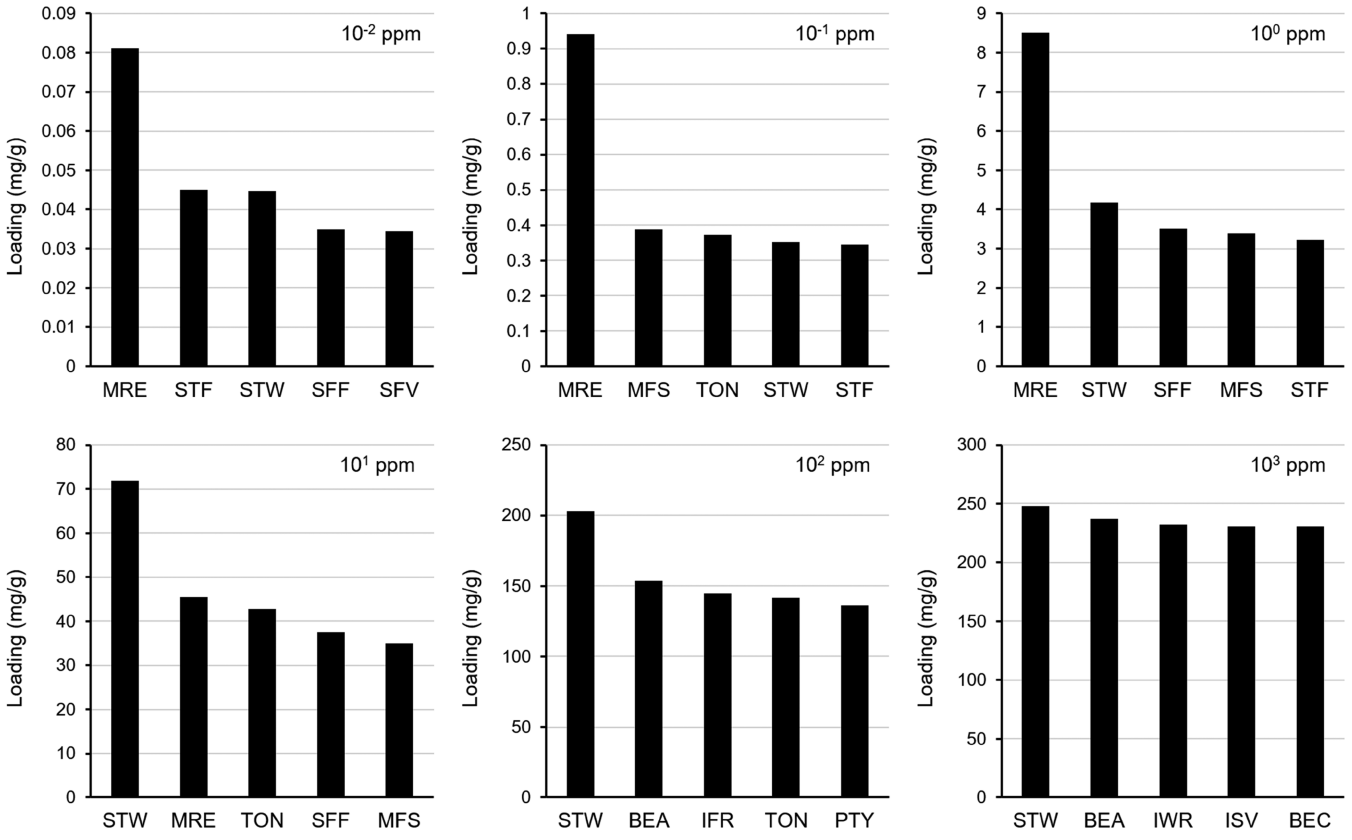

Figure 4. Top five 1-bromopropane adsorbing zeolites at 20 °C within the 10^{-2}–10^{3} ppm ambient concentration range.

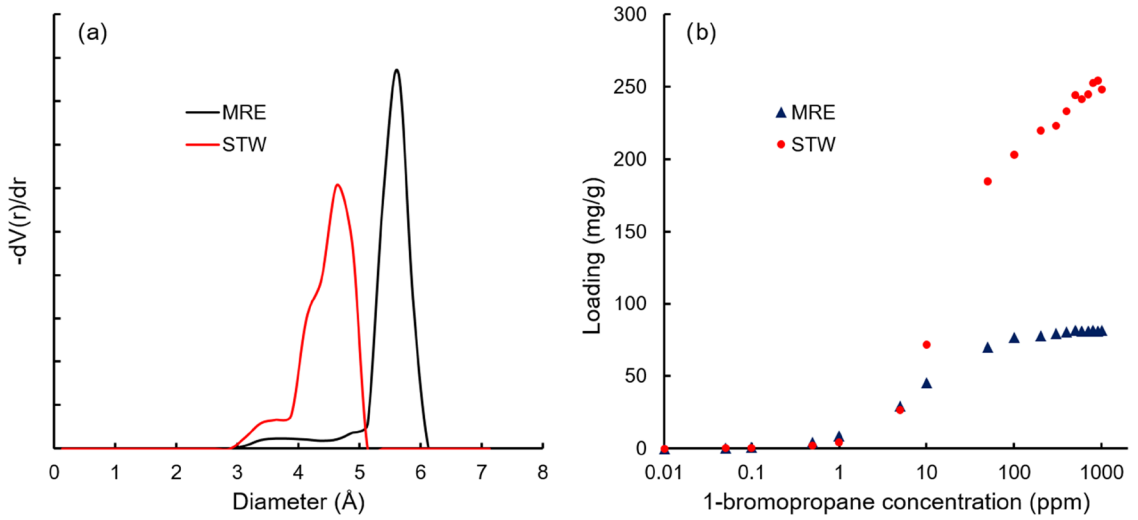

Figure 5. (a) Pore size distributions of MRE and STW zeolites and (b) 1-bromopropane adsorption isotherms of MRE and STW at 20 °C from GCMC simulations.

bromopropane concentrations can be attributed to its 1-dimensional 10-membered ring channel along [100]. This channel is around 5.6 Å in diameter and provides an optimal fit for 1-bromopropane molecules (Figures 5a and S5). STW, on the other hand, has narrower pores; a helical 10-membered ring channel along [001], which is ≈4.6 Å in diameter, and an 8-membered ring channel along ⟨100⟩, which has a diameter of ≈3.6 Å (Figure 5a). However, despite having narrower pores, the intersection of the two channels yields voids that result in a structure, which has a considerably higher accessible specific surface area, 380 vs 175 m^2/g, and pore volume, 0.487 vs 0.188 cm^3/g, compared to MRE. The pores of STW are rapidly filled once the concentration of 1-bromopropane exceeds 10^0 ppm (Figure S6); however, MRE pores are almost saturated around the same concentration at a lower loading (Figure 5b). To the best of our knowledge, there are no experimental data for 1-bromopropane adsorption in zeolites; however, a joint experimental/computational study showed that STW has ∼1.5 times more loading capacity for pentane, hexane, and heptane isomers compared to pure silica MFI at similar pressures considered in this work.[40] For 1-bromopropane, this varies between 1.7 and 5.2 (Table 4), which suggests that 1-

https://doi.org/10.1021/acs.jpcc.2c00086
J. Phys. Chem. C 2022, 126, 5728−5734

bromopropane, which has three carbons, packs more efficiently in STW pores compared to alkanes with higher number of carbons.

Table 4. Ratio of 1-Bromopropane Uptake in STW to that in MFI from GCMC Simulations

1-bromopropane concentration (ppm)	10^{-2}	10^{-1}	10^{0}	10^{1}	10^{2}	10^{3}
STW/MFI uptake ratio	3.1	2.5	3.6	5.2	2.4	1.7

4. CONCLUSIONS

In this work, a united-atom model of 1-bromopropane was developed to investigate its capture in hydrophobic zeolites. VLCC, boiling temperature, critical temperature, critical density, and vapor pressures computed with GEMC simulations using the new model were in excellent agreement with the available experimental data. GCMC simulations carried out for 52 hydrophobic zeolites, which have a PLD larger than 4.0 Å showed that a filtering system that consists of MRE and STW zeolites can capture 1-bromopropane within its ambient concentration range that occurs as a result of its release in various industrial and commercial applications as identified by the US EPA. STW is particularly a promising material for 1-bromopropane capture as it is the only zeolite that appears among the top five performing zeolites for all of the ambient concentration points investigated (Figure 4). In addition to zeolites, there are other porous material types, such as metal−organic frameworks and covalent−organic frameworks, which can demonstrate even higher 1-bromopropane capture capacity. The new united-atom model developed in this work can be used to explore other material types that can help reduce harmful human exposure to 1-bromopropane.

■ ASSOCIATED CONTENT

Supporting Information

The Supporting Information is available free of charge at https://pubs.acs.org/doi/10.1021/acs.jpcc.2c00086.

Partial atomic charges of all atom 1-bromopropane molecule, zeolite force field parameters, snapshots from GCMC simulations, and sample simulation input files (PDF)

GCMC simulation sample (ZIP)

■ AUTHOR INFORMATION

Corresponding Author

A. Ozgur Yazaydin − *Department of Chemical Engineering, University College London, London WC1E 7JE, United Kingdom;* orcid.org/0000-0001-8562-723X; Email: ozgur.yazaydin@ucl.ac.uk

Complete contact information is available at: https://pubs.acs.org/10.1021/acs.jpcc.2c00086

Notes

The author declares no competing financial interest.

■ ACKNOWLEDGMENTS

The author acknowledges the use of the UCL Myriad High Performance Computing Facility (Myriad@UCL) and associated support services in the completion of this work.

■ REFERENCES

(1) Karaffa, L. S. *The Merck Index: An Encyclopedia of Chemicals, Drugs, and Biologicals*; RSC Publishing, 2013.

(2) *Preliminary Information on Manufacturing, Processing, Distribution, Use, and Disposal: 1-Bromopropane*; United States Environmental Protection Agency, 2017.

(3) Blando, J. D.; Schill, D. P.; Cruz, M. P. D. L.; Zhang, L.; Zhang, J. Preliminary Study of Propyl Bromide Exposure among New Jersey Dry Cleaners as a Result of a Pending Ban on Perchloroethylene. *J. Air Waste Manage. Assoc.* **2010**, *60*, 1049−1056.

(4) Center for the Evaluation of Risks to Human Reproduction. Ntp-Cerhr Expert Panel Report on the Reproductive and Developmental Toxicity of 1-Bromopropane. *Reprod. Toxicol.* **2004**, *18*, 157−187.

(5) Majersik, J. J.; Caravati, E. M.; Steffens, J. D. Severe Neurotoxicity Associated with Exposure to the Solvent 1-Bromopropane (N-Propyl Bromide). *Clin. Toxicol.* **2007**, *45*, 270−276.

(6) Liu, F.; Ichihara, S.; Valentine, W. M.; Itoh, K.; Yamamoto, M.; Sheik Mohideen, S.; Kitoh, J.; Ichihara, G. Increased Susceptibility of Nrf2-Null Mice to 1-Bromopropane−Induced Hepatotoxicity. *Toxicol. Sci.* **2010**, *115*, 596−606.

(7) Ichihara, G.; Kitoh, J.; Li, W.; Ding, X.; Ichihara, S.; Takeuchi, Y. Neurotoxicity of 1-Bromopropane: Evidence from Animal Experiments and Human Studies. *J. Adv. Res.* **2012**, *3*, 91−98.

(8) Frasch, H. F.; Dotson, G. S.; Barbero, A. M. In Vitro Human Epidermal Penetration of 1-Bromopropane. *J. Toxicol. Environ. Health, Part A* **2011**, *74*, 1249−1260.

(9) Garner, C. E.; Sloan, C.; Sumner, S.; Burgess, J.; Davis, J.; Etheridge, A.; Parham, A.; Ghanayem, B. Cyp2e1-Catalyzed Oxidation Contributes to the Sperm Toxicity of 1-Bromopropane in Mice. *Biol. Reprod.* **2007**, *76*, 496−505.

(10) *Risk Evaluation for 1-Bromopropane (N-Propyl Bromide)*; United States Environmental Protection Agency, 2020.

(11) Dubbeldam, D.; Calero, S.; Ellis, D. E.; Snurr, R. Q. Raspa: Molecular Simulation Software for Adsorption and Diffusion in Flexible Nanoporous Materials. *Mol. Simul.* **2016**, *42*, 81−101.

(12) Martin, M. G.; Siepmann, J. I. Transferable Potentials for Phase Equilibria. 1. United-Atom Description of N-Alkanes. *J. Phys. Chem. B* **1998**, *102*, 2569−2577.

(13) Jorgensen, W. L.; Maxwell, D. S.; Tirado-Rives, J. Development and Testing of the Opls All-Atom Force Field on Conformational Energetics and Properties of Organic Liquids. *J. Am. Chem. Soc.* **1996**, *118*, 11225−11236.

(14) van der Spoel, D.; van Maaren, P. J.; Caleman, C. Gromacs Molecule & Liquid Database. *Bioinformatics* **2012**, *28*, 752−753.

(15) Caleman, C.; van Maaren, P. J.; Hong, M.; Hub, J. S.; Costa, L. T.; van der Spoel, D. Force Field Benchmark of Organic Liquids: Density, Enthalpy of Vaporization, Heat Capacities, Surface Tension, Isothermal Compressibility, Volumetric Expansion Coefficient, and Dielectric Constant. *J. Chem. Theory Comput.* **2012**, *8*, 61−74.

(16) Frisch, M. J.; Trucks, G. W.; Schlegel, H. B.; Scuseria, G. E.; Robb, M. A.; Cheeseman, J. R.; Scalmani, G.; Barone, V.; Mennucci, B.; Petersson, G. A.; et al. *Gaussian 09*, revision B.01; Gaussian, Inc.: Wallingford, CT, 2009.

(17) Breneman, C. M.; Wiberg, K. B. Determining Atom-Centered Monopoles from Molecular Electrostatic Potentials. The Need for High Sampling Density in Formamide Conformational Analysis. *J. Comput. Chem.* **1990**, *11*, 361−373.

(18) Panagiotopoulos, A. Z. Direct Determination of Phase Coexistence Properties of Fluids by Monte Carlo Simulation in a New Ensemble. *Mol. Phys.* **1987**, *61*, 813−826.

(19) Panagiotopoulos, A. Z.; Quirke, N.; Stapleton, M.; Tildesley, D. J. Phase Equilibria by Simulation in the Gibbs Ensemble. *Mol. Phys.* **1988**, *63*, 527−545.

(20) Poursaeidesfahani, A.; Rahbari, A.; Torres-Knoop, A.; Dubbeldam, D.; Vlugt, T. J. H. Computation of Thermodynamic Properties in the Continuous Fractional Component Monte Carlo Gibbs Ensemble. *Mol. Simul.* **2017**, *43*, 189−195.

(21) Torres-Knoop, A.; Balaji, S. P.; Vlugt, T. J. H.; Dubbeldam, D. A Comparison of Advanced Monte Carlo Methods for Open Systems: Cfcmc Vs Cbmc. *J. Chem. Theory Comput.* **2014**, *10*, 942−952.
(22) Shi, W.; Maginn, E. J. Continuous Fractional Component Monte Carlo: An Adaptive Biasing Method for Open System Atomistic Simulations. *J. Chem. Theory Comput.* **2007**, *3*, 1451−1463.
(23) Baerlocher, C.; M, L. B., Database of Zeolite Structures. http://www.iza-structure.org/databases/ 2017.
(24) Bai, P.; Tsapatsis, M.; Siepmann, J. I. Trappe-Zeo: Transferable Potentials for Phase Equilibria Force Field for All-Silica Zeolites. *J. Phys. Chem. C* **2013**, *117*, 24375−24387.
(25) Sarkisov, L.; Bueno-Perez, R.; Sutharson, M.; Fairen-Jimenez, D. Materials Informatics with Poreblazer V4.0 and the Csd Mof Database. *Chem. Mater.* **2020**, *32*, 9849−9867.
(26) Dubbeldam, D.; Torres-Knoop, A.; Walton, K. S. On the Inner Workings of Monte Carlo Codes. *Mol. Simul.* **2013**, *39*, 1253−1292.
(27) Peng, D.-Y.; Robinson, D. B. A New Two-Constant Equation of State. *Ind. Eng. Chem. Fundam.* **1976**, *15*, 59−64.
(28) Rowlinson, J. S.; Widom, B., *Molecular Theory of Capillarity*; Courier Corporation, 2013.
(29) Rowlinson, J. S.; Swinton, F., *Liquids and Liquid Mixtures: Butterworths Monographs in Chemistry*; Butterworth-Heinemann, 2013.
(30) Sandler, S. I., *Chemical, Biochemical, and Engineering Thermodynamics*; John Wiley & Sons, 2017.
(31) Allen, M. P.; Tildesley, D. J., *Computer Simulation of Liquids*; Oxford University Press, 2017.
(32) Bolotnikov, M. F.; Neruchev, Y. A.; Ryshkova, O. S. Density of Some 1-Bromoalkanes within the Temperature Range from (243.15 to 423.15) K. *J. Chem. Eng. Data* **2007**, *52*, 1065−1068.
(33) Rutherford, W. Viscosity and Density of Some Lower Alkyl Chlorides and Bromides. *J. Chem. Eng. Data* **1988**, *33*, 234−237.
(34) Ryshkova, O.; Neruchev, Y. A. Investigations of the Equilibrium Properties of Liquid Bromoalkanes on the Saturation Curve. *High Temp.* **2009**, *47*, 664−668.
(35) Stull, D. R. Vapor Pressure of Pure Substances. Organic and Inorganic Compounds. *Ind. Eng. Chem.* **1947**, *39*, 517−540.
(36) Rumble, J. R.; Bruno, T. J.; Doa, M. J. *Crc Handbook of Chemistry and Physics: A Ready-Reference Book of Chemical and Physical Data*, 101st ed.; Rumble, J. R.; Bruno, T. J.; Doa, M. J., Eds.; CRC Press/Taylor & Francis Group: Boca Raton, 2020.
(37) Chai, J.-D.; Head-Gordon, M. Long-Range Corrected Hybrid Density Functionals with Damped Atom−Atom Dispersion Corrections. *Phys. Chem. Chem. Phys.* **2008**, *10*, 6615−6620.
(38) Schlenker, J. L.; Rohrbaugh, W. J.; Chu, P.; Valyocsik, E. W.; Kokotailo, G. T. The Framework Topology of Zsm-48: A High Silica Zeolite. *Zeolites* **1985**, *5*, 355−358.
(39) Rojas, A.; Camblor, M. A. A Pure Silica Chiral Polymorph with Helical Pores. *Angew. Chem., Int. Ed.* **2012**, *51*, 3854−3856.
(40) Pérez-Botella, E.; Misturini, A.; Sala, A.; Palomino, M.; Corma, A.; Sastre, G.; Valencia, S.; Rey, F. Insights into Adsorption of Linear, Monobranched, and Dibranched Alkanes on Pure Silica Stw Zeolite as a Promising Material for Their Separation. *J. Phys. Chem. C* **2020**, *124*, 26821−26829.

https://doi.org/10.1021/acs.jpcc.2c00086
J. Phys. Chem. C 2022, 126, 5728−5734